Chinese Chemical Letters 37 (2026) 111841

Contents lists available at ScienceDirect

Chinese Chemical Letters

journal homepage: www.elsevier.com/locate/cclet

The micro-nano electrospinning membrane with water repellenting separation effect for interface hemostasis and anti-adhesion

Xiaojie Sun[a,b,1], Xiaoyan Yang[b,1], Zitong Wang[a], Furui Qu[a], Xin Cong[b], Qingsong Fu[c], Chang Su[b], Xiguang Chen[a,b,e], Kai Shao[c,d,*], Zhiyu He[f,*], Chao Feng[a,b,*]

[a] Sanya Oceanographic Institute, Ocean University of China, Sanya 572024, China
[b] College of Marine Life Science, Ocean University of China, Qingdao 266005, China
[c] Laboratory of Cerebrospinal Fluid Cytology and Neuroimmunology, Department of Central Laboratory, Qilu Hospital (Qingdao), Cheeloo College of Medicine, Shandong University, Qingdao 266035, China
[d] Department of Clinical Laboratory, Qilu Hospital of Shandong University, Ji'nan 250012, China
[e] Laoshan Laboratory, Qingdao 266000, China
[f] Advanced Research Institute of Multidisciplinary Science, Beijing Institute of Technology (BIT), Zhuhai 519088, China

ARTICLE INFO

Article history:
Received 4 June 2025
Revised 12 September 2025
Accepted 15 September 2025
Available online 16 September 2025

Keywords:
Electrospinning hemostatic
Micro-nano structure
Water repellenting separation effect
Interface hemostasis
Anti-adhesion

ABSTRACT

Rapid hemostasis is a paramount issue in tissue wound repair treatment. Currently, hydrophilic hemostatic materials are favored for their absorption concentration capabilities in achieving swift hemostasis. However, the subsequent adherence of these materials to the wound presents another challenge, impacting the overall therapeutic outcome. Here, we reported a flexible electrospinning membrane (75D-P) composed of polyacrylonitrile (PAN) and diatom biosilica (DB), which integrated the submicron-sized pores of fiber membranes with the hierarchical porous structure of DB. It exhibited weak interfacial hydrophobicity, enabling rapid plasma protein adsorption capacity and accelerating blood coagulation at the material interface. The clotting time of kaolin commercial hemostatic agent-QuikClot® (QC) was 200 s, and that of 75D-P was 100 s, with the minimum tissue adhesion (0.06 N). Importantly, in the rabbit injury models, the dosage of the 75D-P was far below that of the QC group, yet it maintained comparable clotting time (about 400 s) and blood loss (4 g). We have integrated DB and PAN in electrospinning membrane could achieve a distinct water repellenting separation effect on blood components, promoting efficient interfacial blood coagulation. These offer insights into facilitating the blood clots formation at interfacial, thereby mitigating excessive material blood absorption and tissue adhesion.

© 2026 Published by Elsevier B.V. on behalf of Chinese Chemical Society and Institute of Materia Medica, Chinese Academy of Medical Sciences.

Trauma represents a pervasive global public health challenge [1–3]. Achieving effective hemostasis is critical in trauma management to reduce preventable mortality [4,5], especially within the "golden 10 min" after injury [6]. The efficacy of hemostatic materials directly impacts rescue outcomes [7,8]. Consequently, these materials function as critical facilitators of the hemostatic process, significantly accelerating coagulation at the bleeding site [9–11].

Although hemostatic materials represented by traditional gauze are widely used in clinical practice [12], they have inherent problems of blood infiltration. Even when augmented with accelerators (*e.g.*, kaolin), these still face various problems with hemostasis [13,14]. For instance, excessive reliance on the absorption-concentration mechanism can consume local blood volume [15–21], dilute coagulation factors, and impair the cascade efficiency [22–24]. Internal hypercoagulation traps clots within the matrix, acting as physical crosslinks that strengthen material-tissue adhesion [25–28]. Moreover, forcibly removing adhered materials may cause secondary trauma, rebleeding, or infection [3,29], while residual fragments risk foreign body reactions, especially in vulnerable populations [30,31].

To address these challenges, electrospinning materials demonstrate unique potential due to tunable structural hierarchy [32,33]. Specifically, electrospinning enables precise control over fiber diameter and inter-fiber pore architecture [34,35], while incorporating inorganic components can modulate surface energy, multi-scale roughness, and porosity [36]. Building on this, we hypothesized that extended electrospinning duration could generate densely packed polyacrylonitrile (PAN) fiber networks with reduced pore connectivity, thereby enhancing topological anti-wetting capabil-

* Corresponding authors.
E-mail addresses: qlshaokai@163.com (K. Shao), hezhiyu@ouc.edu.cn (Z. He), fengchao@ouc.edu.cn (C. Feng).
[1] These authors contributed equally to this work.

https://doi.org/10.1016/j.cclet.2025.111841
1001-8417/© 2026 Published by Elsevier B.V. on behalf of Chinese Chemical Society and Institute of Materia Medica, Chinese Academy of Medical Sciences.

ity [37,38]. However, pure PAN membranes exhibited inherent hydrophilicity (water contact angle: 61.4°) due to polar nitrile groups, which failed to achieve rapid hemostasis. To overcome this, we integrated diatom biosilica (DB), possessing intrinsic micro-nano hierarchical porosity, into the PAN matrix to construct a composite membrane (75D-P). It is worth noting that 75D-P achieves a weakly hydrophobic transition through a synergistic effect, which has a significant interfacial advantage in promoting blood coagulation [39].

Here, we report a 75D-P electrospinning membrane that achieved rapid hemostasis *via* the water repellenting separation effect through three synergistic pathways: (i) The hydrophobic surface of the membrane generated an energy barrier that could suppress longitudinal blood infiltration, establishing a dynamic water-repelling barrier. This effectively confined blood contact to the superficial layer, preventing dilution of coagulation factors. (ii) Hierarchically porous structure of DBs provided high-affinity binding sites for key hemostatic components while simultaneously contributing to the enhanced hydrophobic interfacial characteristics. (iii) Water repellenting separation effect occurred at the material-blood interface. Coagulation components were adsorbed and enriched at the interface region under the combined actions of interfacial adsorption and hydrophobic repulsion. This created a localized hypercoagulable microenvironment that would promote interfacial coagulation while significantly reducing tissue adhesion. The water repellenting separation effect introduced in this study offers a concept for the design of advanced hemostatic materials. It not only challenges our conventional understanding of bleeding control mechanisms but also introduces a fresh perspective from the angle of selective separation and management of blood components.

PAN-DB electrospinning membranes were fabricated by electrospinning PAN solutions containing different DB concentrations (25, 50, and 75 mg/mL), designated as 25D-P, 50D-P, and 75D-P, respectively (Fig. 1a and Fig. S1 in Supporting information). Scanning electron microscope (SEM) images revealed that DB particles were not only embedded within the PAN-DB membranes but also exhibited more uniform dispersion compared to the pure PAN membrane. Some particles were encapsulated by the fibers, while others protruded from the surface, preserving DB's crucial layered porous structure essential for hemostatic functionality (Fig. 1b, Figs. S2 and S3a in Supporting information). Elemental mapping confirmed a uniform distribution of Si elements across all composite membranes (25D-P, 50D-P, 75D-P), contrasting with the absence of Si in the pure PAN membrane (Fig. S3b in Supporting information), attesting to effective DB incorporation into the PAN matrix. The structural variations of the PAN-DB electrospinning membranes were further analyzed through Fourier transform infrared (FTIR). Compared with DBs, new peaks emerged at 2242 cm^{-1} in 25D-P, 50D-P, and 75D-P spectra, corresponding to the characteristic C≡N stretching vibrations of PAN [40]. When compared to PAN, the absorption peaks at 1130 and 464 cm^{-1} (attributed to Si-O-Si bending vibrations) and 959 cm^{-1} (assigned to Si-OH stretching vibrations) appeared in the composite spectra, consistent with characteristic DB peaks (Fig. 1c) [41]. The corroboration of FTIR with above results underscored the successful synthesis of 25D-P, 50D-P, and 75D-P, integrating PAN with DBs through electrospinning.

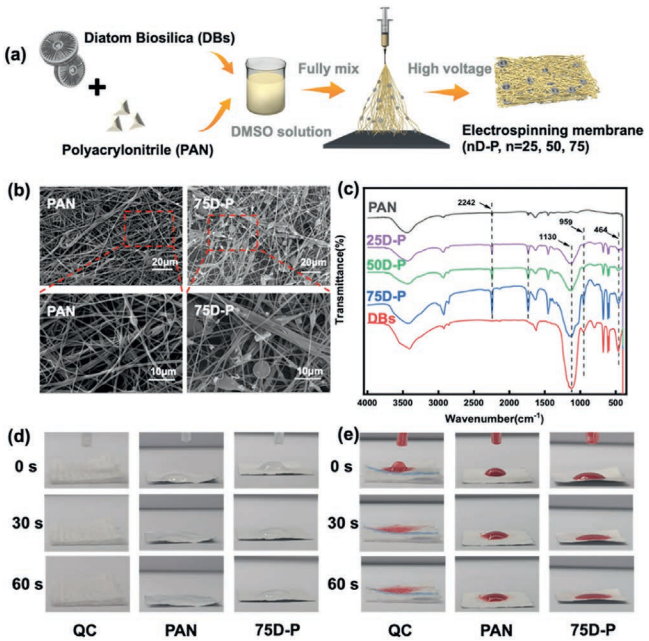


Fig. 1. (a) Preparation of electrospinning solution and diatom biosilica-polyacrylonitrile (D-P) membranes. (b) SEM morphology: PAN (with smooth fibers), 75D-P (DB-modified nanofibers), scales from top to bottom: 20, 10 μm. (c) FTIR spectra: Characteristic DB peaks (959 cm^{-1}) in 25D-P/50D-P/75D-P. (d) Water diffusion: QC (radial spreading) compared with 75D-P/PAN (localized confinement) at 0/30/60 s. (e) Blood diffusion: QC (rapid permeation) compared with 75D-P/PAN at material surface.

The 75D-P electrospinning membranes exhibited a rapid hemostatic effect as shown as Figs. S4 and S5 (Supporting information). To elucidate the hemostatic mechanism of it, we comprehensively investigated material wettability, permeability, and diffusivity toward blood constituents. Given that water is the main liquid component of blood, material-water interactions were primarily examined. The water contact angle of 75D-P measured 89.1° (Fig. S6), close to the hydrophobicity threshold (90°). This near-hydrophobic surface could minimize the solid-liquid interfacial energy, thereby significantly promoting the enrichment and adsorption of coagulation factors at the interface [42,43]. The absorbent liquid results showed that all the tested materials quickly attained water absorption saturation within 1 min (Fig. S7 in Supporting information), and then maintaining a stable water absorption state. Among them, the water absorption of QuikClot® (QC) hemostatic gauze was as high as 993.06% ± 72.67%, while that of 75D-P and PAN were 437.79% ± 9.65% and 240.68% ± 37.21% (Fig. S8a in Supporting information). Compared with PAN, the enhanced water absorption of 75D-P over PAN could be attributed to the micron sized DBs, which could further enrich the pore structure of the electrospinning membranes, resulting in increased water absorption. In addition, the results of blood absorption experiment showed that QC, PAN and 75D-P all reached blood absorption saturation within 2 min. Similarly, QC again led the way with a blood absorption ration exceeding 562.3%, while 75D-P had a lower blood absorption ration of 120.4% (Fig. S8b in Supporting information). It is noted that compared with the higher water absorption and blood absorption of QC, 75D-P did not rely on the absorption concentration effect of blood or water, and still demonstrated a rapid hemostatic effect (Fig. S9 in Supporting information). We speculated that 75D-P might have different mechanisms for blood components and water, which also could give it the ability to stop bleeding quickly.

To characterize surface wetting behavior, water and blood droplets were deposited on each material. QC exhibited rapid absorption of both fluids, while PAN and 75D-P demonstrated distinct wetting resistance (Figs. 1d and e). It is worth noting that PAN maintained consistent hemophobicity (Fig. 1e), while 75D-P tended to progressive blood spreading across its surface, evidenced by increasing wetted area over time. This highlighted 75D-P's unique interfacial behavior combining wetting resistance with directional fluid transport. This unique interfacial blood behavior stems from the synergistic physicochemical properties: On the one hand, the inherent micro-nano pore structure of 75D-P, according to the Laplace equation ($\Delta P = 2\gamma\cos\theta/r$), can generate a significant

capillary pressure (ΔP), which can effectively resist liquid penetration. On the other hand, the comparison of PAN and 75D-P under the same spinning time/pore size (Fig. S6) indicated that, after excluding the dominant factor of pore size, the introduction of DBs ccould improve the water repellency property of the material surface to a certain extent.

The results of a blood dripping experiment revealed interesting phenomena on blood diffusivity and permeability across the electrospinning membranes' surface. Specifically, the blood diffusivity area of the 75D-P-3 group exhibited no significantly deviation from that of the 75D-P-1 and 75D-P-2 groups, all of which rapidly expanded within 1 min (Fig. S10a in Supporting information). Conversely, the blood diffusivity area of the 75D-P-4 group was markedly reduced, suggesting inferior blood diffusivity. The permeation and diffusion results showed that 75D-P-3 achieved blood permeation and diffusion within 1–5 min, whereas 75D-P-1 and 75D-P-2 exhibited incomplete permeation and diffusion even after 20 min of experimentation. And 75D-P-4 demonstrated rapid blood permeation within 1 min (Fig. S10b in Supporting information). It is noting that the longitudinal permeability of PAN-DB electrospinning membranes varied significantly with the increase of spinning time, with the superior longitudinal permeability and diffusion observed with 3 h spinning times. Collectively, these findings indicated that 75D-P-3 have possessed favorable blood diffusivity, permeability, and liquid wettability.

Quantitative assessments showed that the protein adsorption capacity of plasma protein by 75D-P (>100 mg/g) was significantly higher than that of gauze (GU) (lower than 25 mg/g) and PAN (60 mg/g) (Fig. S11 in Supporting information). The capillary pressure (high ΔP) generated by the micro-nano structure of 75D-P, combined with the functionalized surface of DBs, synergically achieved the hydrophobic behavior and the adsorption and enrichment of plasma proteins by 75D-P on the surface of the blood contact membrane, ultimately achieving rapid hemostasis. This is different from traditional gauze, which relies on millimeter-sized macropores (with capillary pressure close to 0) for passive and rapid absorption.

The pressure environment of the bleeding was further simulated, and the membrane contact results showed that 75D-P exhibited an identical blood anti-permeation behavior as PAN upon contact with the simulated blood flow, with no observable blood dripping within the 1 min (Video S1 in Supporting information). In contrast, GU immediately passed the blood flow, and after its passage through GU, the blood with clotting protein encountered the bicinchoninic acid protein kit (BCA) working fluid beneath, promptly causing a change from blue to a purple (Fig. 2a and Video S2 in Supporting information). Upon completion of the experiment, the examination of the blood distribution on the material surfaces revealed that the 75D-P membrane displayed a uniform blood diffusion pattern across its surface, in accordance with the blood diffusion behavior observed with GU (Fig. 2a). Conversely, PAN exhibited a localized blood distribution, restricted solely to the areas in contact with the syringe (Video S3 in Supporting information), suggesting a deficiency in blood component diffusion capabilities.

The confocal layer scanning outcomes revealed a distinctive behavior among the tested materials. Specifically, the fluorescently tagged plasma protein was added on the 7 layers GU material, it showed uniform diffusion and penetration of green fluorescent labeled protein, highlighting its permeability. In contrast, the 7 layers PAN displayed negligible green fluorescence labeled protein, indicating that the PAN would not make the plasma protein components vertically penetrate. It is noting that the 7 layers of 75D-P material group showed a small amount of green fluorescence, and the fluorescence intensity was relatively reduced and uneven, but the 1 layer of 75D-P showed uniform diffusion and penetration of green fluorescence, and the fluorescence intensity was basically

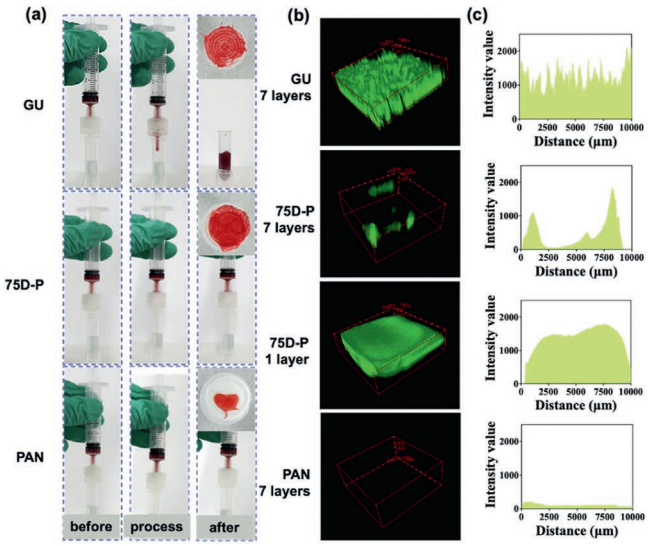


Fig. 2. (a) Blood material interface dynamics: GU (permeation → BCA purple shift) *vs.* 75D-P/PAN (surface retention). Surface of the material: 75D-P showed GU-like diffusion *vs.* PAN's complete confinement. (b, c) Confocal Z-stack analysis: green-fluorescent plasma protein distribution in materials. GU: full penetration; PAN: no penetration; 75D-P: partial penetration; 1-layer 75D-P ≈ 7-layer GU.

consistent with GU. The significant differences between monolayer adsorption (Fig. S11 in Supporting information) and multilayer permeation (Figs. 2b and c), as well as the comparison between surface distribution and deep permeation, jointly reflect the scale dependence of the pore effect. When polyacrylonitrile layers are stacked, nanoparticle clogging dominates fluid resistance (resulting in the anti-permeability of PAN and 75D-P multilayers), while the behavior of monolayer is controlled by surface chemistry (determining the surface diffusion capacity of 75D-P). 75D-P exhibited a certain surface diffusion ability in monolayer (facilitating contact with coagulation proteins), while in multilayer, it showed an anti-permeation ability similar to that of PAN (limiting excessive blood absorption). This distinction conforms to Laplace's principle: the multilayer structure could amplify its inherent impermeability through a composite capillary pressure.

Further SEM observation was conducted on the surface of the material after hemostasis, it showed that a densely fibrin network was congregated and adhering to the surface of the 75D-P membrane. This fibrin network enveloped and adhered to a substantial quantity of red blood cells (RBCs), in stark contrast to the significantly less adhesion of RBCs observed on the QC surface. Furthermore, the adhesion of RBCs to the surface of the DBs exhibited an increasing trend (Fig. 3a). 75D-P actively induced the formation of a dense fibrin network, achieving encapsulation and aggregation of RBCs, thereby accelerating thrombin reactions and platelet activation/aggregation. This fibrin network simultaneously would act as a physical barrier, significantly enhancing the overall density and viscoelastic strength of the clot, and strengthening its ability to resist blood flow shear force and fibrinolysis. Ultimately, it is reflected in the synergistic enhancement of coagulation efficiency and stability. This outstanding performance stems from the synergistic effect of capillary force and DBs interface properties generated by the unique micro-nano stratified pore structure of 75D-P: On the one hand, this effect endowed the material interface with hydrophobicity; on the other hand, it enhanced the adsorption and adhesion of functional components such as coagulation proteins at the interface. The above mechanisms work together to systematically explain the optimal procoagulant performance of 75D-P.

The influence of 75D-P on intrinsic and extrinsic pathway were examined by activated partial thromboplastin time (aPTT) and pro-

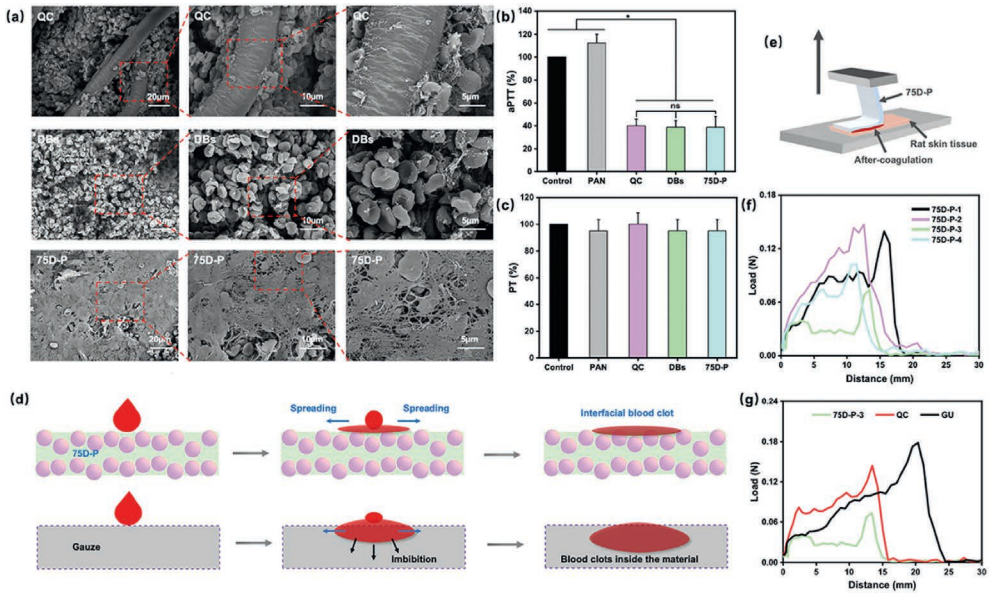


Fig. 3. (a) SEM pictures: 75D-P formed dense fibrin networks encapsulating RBCs *vs.* QC/DBs controls. (b, c) aPTT and PT assays: 75D-P could shorten aPTT to activate intrinsic pathway, with PT unchanged of PAN/DBs. Data are presented as mean ± standard deviation (SD) ($n = 3$). $^*P < 0.05$. ns, no significant difference. (d) Interfacial diagram: the weak hydrophobicity of 75D-P enabled water to diffuse laterally, enriching blood components at the interface. The hydrophilic gauze allowed these components to permeate longitudinally and disperse laterally. (e) Mechanical peeling test: to quantify tissue adhesion after hemostasis. (f, g) Adhesion strength: 75D-P-3 showed minimal peeling force (0.08 N) *vs.* QC, GU, 75D-P-1/2/4.

thrombin time (PT). Compared with the control group, the aPTT values of 75D-P, DBs, and QC were significantly shortened to about 40 %, indicating an acceleration of the intrinsic coagulation pathway. While the PAN group was slightly prolonged in aPTT (Fig. 3b), suggesting a potential delay in this pathway. In contrast, PT results showed that PAN, DBs, and 75D-P had no significant effects on extrinsic pathway (Fig. 3c). These confirmed the specific activation of the intrinsic pathway by DBs within the 75D-P matrix, which could be attributed to the unique negative charge properties of DBs that facilitate the activation of crucial clotting factors [44].

In delving into the rapid hemostasis mechanisms achieved by the 75D-P, we have focused on its water repellenting effect different from the traditional absorption concentration effect. Firstly, the 75D-P membrane exhibited pronounced water repellenting separation effect and controlled hemophobicity, distinguishing it from traditional materials like GU. This interfacial property could diffuse the moisture liquid laterally at the interface of the hemostatic, preventing rapid and excessive penetration of blood into the material, thereby reducing unnecessary blood loss (Fig. 3d). Furthermore, its inherent water insolubility could ensure structural integrity in the body's intricate wet environment, avoiding performance degradation due to dissolution or material residue, thereby guaranting its reliability as a hemostatic agent. Secondly, 75D-P showed interface adsorption effects on blood components such as coagulation proteins, thanks to its designed micro-nano pore distribution. This not only achieved the separation of coagulation function components from water at the 75D-P's interface, but also greatly accelerated the concentration and activation of coagulation factors, creating favorable conditions for the origination and acceleration of the coagulation process (Fig. 3d). Finally, the DB component in 75D-P, with its unique micro-nano level porous structure, could not only enhance the anti-wettability of the material [45], but also effectively promote the separation between coagulation components and water by a large number of surface energy "traps" [46]. This water repellenting separation effect could form blood clots at the wound-material interface, not only alleviating the problem of excessive blood absorption common in traditional hemostatic materials, but also fundamentally solving the tendency of hemostatic-tissues adhesion.

To investigate the adhesion properties of 75D-P after hemostasis, we designed a 90° peeling experiment between materials and tissues (Fig. 3e). Initial results revealed that the 75D-P-3 group required the least peeling force. In contrast, the peeling force for the 75D-P-1, 2, and 4 groups were significantly increased. Specifically, the 75D-P-3 exhibited a minimal peeling force of 0.06 N, representing a reduction compared to the other 75D-P groups (0.12 N), which required twice the force to achieve tissue detachment after hemostasis (Fig. 3f). Subsequently, the 75D-P-3 was compared with QC and GU counterparts. The results demonstrated that the required peeling force for the GU and QC group reached 0.18 N, more than double that of the 75D-P-3 group (Fig. 3g). These findings further indicated that the designed micro-nano structure of the 75D-P-3 electrospinning membranes could facilitate rapid hemostasis while avoiding tissue adhesion through the water repellenting separation effect. Prior to evaluating *in vivo* hemostatic efficacy, we systematically assessed the biosafety of 75D-P. The material exhibited excellent hemocompatibility and cytocompatibility, as evidenced by a hemolysis ratio below 5 % (Fig. S12 in Supporting information) and a cell viability exceeding 85 % (Fig. S13 in Supporting information).

To systematically evaluate the hemostatic efficacy of 75D-P in rats, we established rat tail amputation and liver injury models (Figs. 4a and e). All animal experiments were approved by the Animal Ethics Committee of Ocean University of China and conducted in accordance with relevant guidelines to ensure animal welfare. In the rat tail amputation model, 75D-P showed excellent hemostatic performance (Fig. 4b), with the shortest coagulation time (84 ± 10.39 s) and the least blood loss (191 ± 66.81 mg). This advantage could be attributed to its distinctive water repellenting separation effect, facilitating prompt contact of blood components with porous DBs, thereby accelerating the initiation of the clotting cascade. In contrast, traditional gauze materials tend to absorb excessive blood (the blood loss was over 2500 mg), slowing down the clotting process (the clotting time was over 310 s). While the

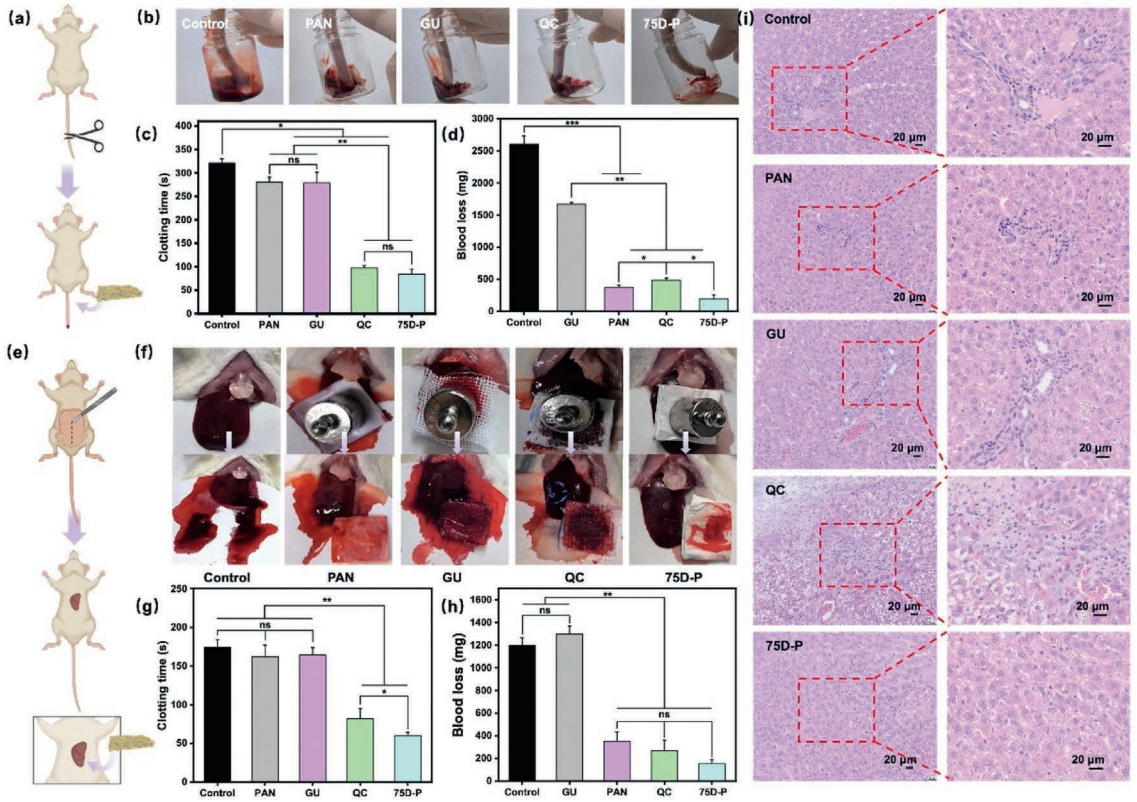


Fig. 4. Model validation of rapid hemostasis and *in vivo* biocompatibility. (a) Surgical schematic. (b) Hemostasis visualization. (c) Clotting time: 75D-P (84 s) *vs.* control (over 310 s). (d) Blood loss: 75D-P (191 mg) lower than GU (over 2000 mg). (e) Surgical schematic. (f) Hemostasis visualization. (g) Clotting time: 75D-P < GU. (h) Blood loss: 75D-P < GU. (i) H&E histopathology (day 3): 75D-P showed comparable hemostasis to QC without inflammatory infiltration, necrosis, or fibrosis (compared with control). Scale bar: 20 μm. Data are presented as mean ± SD ($n = 5$). $^{*}P < 0.05$, $^{**}P < 0.01$, $^{***}P < 0.001$.

QC group (the clotting time was 97.33 ± 5.03 s) demonstrated some reduced clotting time, its blood loss was substantially higher, amounting to 483 ± 35.59 mg (Figs. 4c and d). Additionally, although the blood loss in the PAN group was significantly reduced, the hemostasis time was not significantly shortened. This indicates that although the hydrophobic properties of PAN nanofibers could moderately slow down blood loss, the prolonged clotting time stems from the absence of DB's key coagulation component separation and concentration effect.

Furthermore, the rat liver injury model's results showed that the clotting time of the 75D-P group (59.67 ± 4.51 s) was shortened compared with that of the control group (174.33 ± 10.02 s), and was also superior to that of the commercial QC group (82 ± 113.08 s), which showed a 27.23 % reduction (Figs. 4f and g). This significantly shortening of the clotting time suggested that the high efficacy of 75D-P in controlling visceral bleeding. At the same time, in terms of blood loss, the 75D-P group (154 ± 34.12 mg) exhibited an 88.15 % reduction compared to the GU group (1299.33 ± 71.25 mg), effectively preventing the potential life threat caused by massive blood loss (Fig. 4h). The histopathological analysis of hematoxylin and eosin (H&E) staining revealed that compared with the control group, the common gauze GU group and the commercial hemostatic agent QC group, there was no obvious inflammatory cell infiltration, tissue necrosis or fibrosis in the 75D-P group (Fig. 4i). The 75D-P showed rapid coagulation and low blood loss in both rat tail amputation models and liver injury models, thoroughly validating its significant advantages and effectiveness *in vivo* hemostatic applications. To assess the effectiveness of 75D-P in large animals, as shown in Fig. S14 (Supporting information), healthy New Zealand white rabbits underwent modeling procedures to simulate liver injury and femoral artery/vein bleeding (Figs. S14a and f). When compared to the QC group, the 75D-P group exhibited comparable clotting times (Figs. S14c and h) and blood loss volumes (Figs. S14d and i). It is worth noting that despite demonstrating equivalent hemostatic efficacy, the 75D-P group utilized significantly less material compared to the QC gauze (Figs. S14b and g). Furthermore, after hemostasis, tissues were collected from the wound sites of the rabbits for inductively coupled plasma mass spectrometry (ICP-MS) analysis. The results revealed no significant increase in the distribution of the Si element at the wound site following the application of 75D-P, compared to the control group.

In summary, we have fabricated a 75D-P electrospinning membrane with micro-nano structures using the electrospinning technique. DBs were homogeneously distributed throughout the PAN nanofibers. The dense pore structure size, in combination with the characteristics of DBs, jointly endowed the material with hydrophobicity. When the 75D-P upon contact with wound blood, it exerts the water repellenting separation effect: The hydrophobic surface effectively would direct the majority of blood water away, preventing its infiltration, thereby minimizing blood loss. Meanwhile, DBs promotes the adsorption and enrichment of functional blood components such as coagulation proteins at the interface. This mechanism enabled 75D-P to precisely regulate the formation of interfacial blood clots and achieve rapid interfacial hemostasis of wounds, avoiding to excessive tissue blood loss. From the perspective of precise separation of blood components at the material-wound interface, it reveals the physicochemical basis for achieving efficient and controllable hemostasis.

Declaration of competing interest

The authors declare that they have no known competing financial interests or personal relationships that could have appeared to influence the work reported in this paper.

CRediT authorship contribution statement

Xiaojie Sun: Data curation, Conceptualization. **Xiaoyan Yang:** Writing – original draft, Data curation, Conceptualization. **Zitong Wang:** Investigation. **Furui Qu:** Software, Investigation. **Xin Cong:** Software, Data curation. **Qingsong Fu:** Formal analysis, Data curation. **Chang Su:** Data curation. **Xiguang Chen:** Supervision. **Kai Shao:** Writing – review & editing, Supervision, Investigation. **Zhiyu He:** Supervision, Resources, Project administration. **Chao Feng:** Writing – review & editing, Supervision, Resources, Project administration, Funding acquisition.

Acknowledgments

The work was supported by National Natural Science Foundation of China (Nos. 82172095, 82471429), Natural Science Foundation of Shandong Province (No. ZR2024MH013), Qingdao Key Technology Research and Industrialization Demonstration Project (No. 23–1–3-hysf-1-hy), Sanya Science and Technology Special Fund (No. 2022KJCX57), Education Department of Hainan Province (No. Hnjg2024–276), Sanya Science and Technology "Star" Special Research Project (No. 2024KJFX030), and China Postdoctoral Science Foundation General Program (No. 2025MD774144), Postdoctoral Research Project of Hainan Province (No. 103000–112255509).

Supplementary materials

Supplementary material associated with this article can be found, in the online version, at doi:10.1016/j.cclet.2025.111841.

References

[1] G. Chen, Y. Yu, X. Wu, et al., Adv. Funct. Mater. 28 (2018) 1801386.
[2] Y. Jiang, J. Wang, H. Zhang, et al., Sci. Bull. 67 (2022) 1776–1784.
[3] H. Wang, Y. Zhu, L. Zhang, et al., Chin. Chem. Lett. 33 (2022) 2937–2941.
[4] X.F. Li, P. Lu, H.R. Jia, et al., Coord. Chem. Rev. 475 (2023) 214823.
[5] M. Mecwan, J. Li, N. Falcone, et al., Regen. Biomater. 9 (2022) rbac063.
[6] H.H. Versteeg, J.W. Heemskerk, M. Levi, et al., Physiol. Rev. 93 (2013) 327–358.
[7] S. Pourshahrestani, N.A. Kadri, E. Zeimaran, et al., Biomater. Sci. 7 (2019) 31–50.
[8] R.L.J. Zwinkels, H. Endeman, S.E. Hoeks, et al., J. Crit. Care 56 (2020) 288–293.
[9] A.M. Behrens, M.J. Sikorski, P. Kofinas, J. Biomed. Mater. Res. A 102 (2014) 4182–4194.
[10] R.L. Gruen, K. Brohi, M. Schreiber, et al., Lancet 380 (2012) 1099–1108.
[11] A. Malik, F.U. Rehman, K.U. Shah, et al., J. Biomed. Mater. Res. B: Appl. Biomater. 109 (2021) 1465–1477.
[12] B. Wu, F. Du, A. W, et al., Chin. Chem. Lett. 33 (2022) 703–713.
[13] X. Sun, J. Li, K. Shao, et al., Int. J. Biol. Macromol. 182 (2021) 2097–2107.
[14] P. Slezak, C. Keibl, H. Redl, et al., J. Investig. Surg. 33 (2020) 828–838.
[15] S. Chen, R. Li, X. Li, et al., Adv. Drug Deliv. Rev. 132 (2018) 188–213.
[16] S. Chen, J.V. John, A. McCarthy, et al., J. Mater. Chem. B 8 (2020) 3733–3746.
[17] R. Wibel, D.E. Braun, L. Hammerle, et al., Biomacromolecules 22 (2021) 3980–3991.
[18] H. Li, F. Cheng, C. Chavez-Madero, et al., Int. J. Biol. Macromol. 134 (2019) 56–62.
[19] K.L. Aya, R. Stern, Wound Repair Regen. 22 (2014) 579–593.
[20] E. Lih, J.S. Lee, K.M. Park, et al., Acta Biomater. 8 (2012) 3261–3269.
[21] G. Basadonna, Prehosp. Disaster Med. 27 (2012) 217.
[22] J. Li, X. Sun, K. Zhang, et al., Adv. Healthc. Mater. 9 (2020) 2000951.
[23] J. Borges-Vilches, T. Figueroa, S. Guajardo, et al., Colloids Surf. B: Biointerfaces 206 (2021) 111941.
[24] O. Goncharuk, O. Korotych, Y. Samchenko, et al., Mater. Sci. Eng. C 129 (2021) 112363.
[25] M.B. Dowling, R. Kumar, M.A. Keibler, et al., Biomaterials 32 (2011) 3351–3357.
[26] Y. Guo, M. Wang, Q. Liu, et al., Theranostics 13 (2023) 161–196.
[27] H.E. Achneck, B. Sileshi, R.M. Jamiolkowski, et al., Ann. Surg. 251 (2010) 217–228.
[28] B.S. Kheirabadi, J.E. Mace, I.B. Terrazas, et al., J. Trauma Acute Care Surg. 68 (2010) 269–278.
[29] M. Mutignani, T. Seerden, A. Tringali, et al., Gastrointest. Endosc. 71 (2010) 856–860.
[30] E. Spaziani, A. Di Filippo, P. Francioni, et al., Acta Chir. Belg. 118 (2018) 48–51.
[31] G. Franceschini, Carbohydr. Polym. 216 (2019) 213–216.
[32] D.B. Khadka, D.T. Haynie, Nanomedicine 8 (2012) 1242–1262.
[33] H. Zhong, Z. Zhang, M. Wang, et al., Biomater. Sci. 13 (2025) 697–710.
[34] H. Zhong, J. Huang, M. Luo, et al., Nano Res. 16 (2022) 599–612.
[35] H. Zhong, J. Huang, J. Wu, et al., Nano Res. 15 (2021) 787–804.
[36] X. Gao, S. Han, R. Zhang, et al., J. Mater. Chem. B 7 (2019) 7075–7089.
[37] D. Gao, S. Guo, Y. Zhou, et al., J. Colloid Interface Sci. 613 (2022) 396–405.
[38] Lin Feng, Shuhong Li, Huanjun Li, et al., Angew. Chem. Int. Ed. 41 (7) (2002) 1221–1223.
[39] L.C. Xu, J.W. Bauer, C.A. Siedlecki, Colloids Surf. B: Biointerfaces 124 (2014) 49–68.
[40] A. Mollahosseini, M. Rastegari, M. Panahi-Dehghan, J. Chromatogr. Sci. 60 (2022) 401–407.
[41] Z. Cao, C. Su, X. Sun, et al., Carbohydr. Polym. 296 (2022) 119975.
[42] A. Schrauth, Structured Surfaces for Hemocompatibility, Massachusetts Institute of Technology, 2005 Masters Thesis.
[43] M.B. Gorbet, M.V. Sefton, Review: Biomaterial-associated thrombosis: Roles of Coagulation factors, complement, Platelets and Leukocytes, in: D.F. Williams, The Biomaterials: Silver Jubilee Compendium (Eds.), Elsevier Ltd., Oxford, 2006, pp. 219–241.
[44] C. Feng, J. Li, G.S. Wu, et al., ACS Appl. Mater. Interfaces 8 (2016) 34234–34243.
[45] Y.X. Huang, Z. Wang, D. Hou, et al., J. Membr. Sci. 531 (2017) 122–128.
[46] Y. Si, Q. Fu, X. Wang, et al., ACS Nano 9 (2015) 3791–3799.